A study of the abrasive wear behavior of laser-clad tool steel coatings

Wang, Sheng-Hui; Chen, Jianyin; Xue, Lijue

Publisher's version / Version de l'éditeur:
https://doi.org/10.1016/j.surfcoat.2004.10.125
Surface & Coatings Technology, 200, 11, pp. 3446-3458, 2006-03-15

Paper submitted to "Surface and Coatings Technology"

A study of the abrasive wear behaviour of laser-clad tool steel coatings

S.-H. Wang, J.-Y. Chen, L. Xue
Integrated Manufacturing Technologies Institute, National Research Council,
800 Collip Circle, London, Ontario, Canada N6G 4X8

Abstract

A comparative study of the abrasive wear behaviour has been conducted on several tool steel coatings that were deposited by laser cladding process using a CW CO_2 laser in combination with a blown powder feed technique. The laser-clad CPM 15V and CPM 10V coatings exhibit superior abrasive wear resistance as compared with the reference material, AISI D2 tool steel. In contrast, the wear resistance of the CPM 9V and M4 coatings is inferior to that of the D2 steel. As multiple overlapping clad-tracks are used to produce a coating covering relatively large area, a thin layer of a pre-deposited clad-track will be "over-heated" while depositing the next adjacent one. Depending on the coating material, this re-heated zone can exhibit different wear rate compared with the other area of the track in the as-clad condition, which is especially significant for the CPM 10V coating. For coatings with a large proportion of retained austenite, post heat-treatment promotes the transformation of the retained austenite to martensite, improving the wear resistance. The wear resistance of tool steel coatings is dependent upon the matrix microstructure and the features of dispersed carbides, such as their type, proportion, shape, size, and distribution.

(*Keywords*: [C] Laser cladding; [X] Tool steel; [B] Abrasive wear test; [B] Scanning electron microscopy; [B] X-ray diffraction)

1. Introduction

Laser cladding using a blown powder feeding technique is commonly used to produce metallurgical dense coatings on components to improve their corrosion, wear and other surface-related properties [1-8]. During the process, a focused laser beam is irradiated onto a substrate to form a melt pool. The clad material in powder form is delivered into the melt pool by using a carrier gas and is melted due to the high-energy intensity of the laser beam. With the beam being scanned away from the location, the molten material solidifies rapidly to form a solid bead and, consequently, a clad track. Multiple overlapping clad-tracks are needed to form a coating on a large component. In addition to metallurgical bonding between the coating and the substrate, the dilution of the laser-clad layer with elements from the substrate can be controlled to a low level. That is, foreign elements from the substrate can be limited to mix into the coating, preventing undesired deterioration of the inherent properties, such as corrosion and wear resistance, of the coating material.

Tool steels are commonly used for manufacturing moulds, dies and other components that are subjected to extremely high load, to provide the required wear resistance. Group D tool steels containing high carbon and chromium, for example, are widely used for making rolls, forming dies, burnishing tools and other components for cold working applications. Nevertheless, components made of tool steels, especially large ones, are relatively expensive, due to either the material cost or the fabrication expense. On the other hand, because of the requirement for certain bulk material properties (e.g., high toughness), it is sometimes unsuitable to fabricate the entire component with high-alloy tool steel. Therefore, from either economical or functional point of view, there are many cases where it is beneficial to fabricate components using inexpensive, easy-to-fabricate carbon steels, with their wear resistance improved by laser cladding of high-alloy tool steels.

Comparatively, there have been more studies conducted on laser surface melting of tool steels [9-21] as compared with laser cladding [22-24]. The former process is reported to be the most intensively investigated method of laser surface modification on tool steels [25]. The microstructures of laser-surface-melted and laser-clad layers can be similar depending on the cooling rate (if the dilution effect by laser cladding is negligible). In both cases the solidification rate is very high due to rapid self-quenching induced by the large mass of the substrate. Normally, however, laser surface melting correlates with higher cooling rate. The laser processed surface layers generally exhibit fine cellular and/or dendrite structure with uniformly distributed tiny carbides. The matrix may contain martensite, retained austenite and, in some cases, retained δ-ferrite. If the primary phase during solidification is δ-ferrite, it can be retained to room temperature, as observed in laser-surface-melted and laser-clad M2 steel [16-22]. Otherwise, if γ or a carbide is the primary solidification phase, only retained austenite can be achieved. Even in the case where the δ-ferrite should be the primary solidification phase during a normal solidification course, a transition from δ to γ as the primary solidification phase can occur as a result of the high solidification rate during laser surface melting [12, 13], and up to one hundred percent of retained austenite can be obtained when the cooling rate is sufficiently high [12-14]. The retained austenite leads to a relatively low hardness, which can be enhanced by post heat-treatment that promotes the transformation of the retained austenite to martensite and the precipitation of fine carbides [14, 15].

For laser cladding of high-alloy tool steels, cracking often occurs in the coating as a result of thermal and/or phase-transformation stresses. That restricts the applications of these tool steels in laser cladding. Pre-heating of the matrix can be used to eliminate cracking of the coating [26]. Nevertheless, this reduces the cooling rate and, thus, affects the microstructure of the cladding.

Recently, a group of high vanadium-containing tool steels (such as CPM 9V, 10V and 15V) produced for powder metallurgy application has proven to be successful in achieving excellent wear resistance [27-33]. That makes them potential candidates as cladding materials for anti-wear applications. In fact, studies have been reported on laser cladding with CPM 10V [23] and other high vanadium tool steels [24]. Generally, however, there have been few publications focusing upon the investigation of the microstructures and their influences on the wear behaviour of these claddings. The objective of this paper is, therefore, to conduct a comparative study of abrasive wear behaviour of various laser-clad coatings of CPM 9V, 10V and 15V as well as M4 tool steels, and to investigate the effects of the microstructure of the coatings on their wear resistance.

2. Materials and Experimental Details

The materials used for laser cladding were CPM 9V, 10V and 15V as well as M4 tool steel powders. The powders were in spherical shape with an average diameter of 45 μm for CPM 9V, 10V, 15V, and 22 μm for M4. The substrates used for the cladding were AISI 1070 carbon steel plates with a thickness of about 12.5 mm. The nominal compositions of the materials are listed in Table I.

The laser cladding was conducted using a 3kW CW CO_2 laser, in combination with a computer numerically controlled 3-axis motion stage and a powder feeding system using argon as the carrier gas. The substrate was preheated to 200°C to prevent cracking of the coating. Multi-track cladding with desired overlap ratio was made to create the test specimens. The processing parameters are briefly summarized in Table II. The coating covered an area of 55mm×35mm. A second clad layer was deposited on the top of the first one. The total thickness of the coating was about 2 mm, enabling the evaluation of the wear behaviour of the coating without experiencing any effect of dilution at the interface between the coating and the substrate. In fact, the wear occurred mainly within the top layer of the cladding.

All the specimens for wear testing were surface-ground. Wear tests were conducted on the coatings either in as-clad condition or after post heat-treatment, during which the specimens were held at a desired temperature (190, 260, 330, 400, and 600°C, respectively) for two hours with a box furnace followed by furnace cooling. The post heat treatment was conducted primarily in relation to our ongoing study of its influence upon the residual stress of the claddings [34]. In addition to the coatings, D2 tool steel samples (see Table I for the composition), hardened as specified by ASTM Standard G65-94, were also tested as a reference material. The density for the commercially available bulk material is 7.46, 7.41, 7.25, 8.16, 7.8 g/cm^3 for CPM 9V, 10V, 15V, M4 and D2, respectively. One specimen for each condition of the coating and six for D2 reference material were tested.

Abrasive wear tests were conducted using a Falex dry sand/rubber wheel test machine as per the specified procedure A of ASTM Standard G65-94. During the testing, AFS 50-70 testing sand of

rounded quartz from U.S. Silica Company, as specified by the standard, was continuously fed between the specimen and a rubber-rimmed wheel, with a flow rate of 326 g/min. The wheel outer layer of chlorobutyl rubber has a hardness of Durometer A60.5. The rate of the wheel revolution is about 200 rpm during the testing. The abrasion direction was parallel to the direction of the clad tracks. The force used against the specimen was maintained at 130 N during the test. After 6000 wheel revolutions, the mass loss was measured using an analytical balance with a sensitivity of 0.0001 g. The volume loss was then calculated based on the mass loss and the density of the coating material. Because of the slight variation in the diameter of the rubber wheel (from 227.4 to 228.5 mm), the reported volume loss was adjusted one that would be produced by a 228.6-mm diameter wheel, according to ASTM Standard G65-94.

Based on the adjusted volume loss (V_w), the wear resistance (R_w) is defined as [35]:

$$R_w = \frac{SN}{V_w} \tag{1}$$

where N is the normal load, and S is the adjusted lineal distance of the wear path (i.e. 4309 m for the present study).

The microstructure of the specimens was observed using an optical microscope as well as a scanning electron microscope (SEM). Energy-dispersive X-ray spectroscopy (EDS) was used to analyze local chemical compositions. X-ray diffraction (XRD) phase identification was conducted by using a Philips X'Pert system, with Cu K_α operated at 40 kV/45 mA. Based on the diffraction patterns, the relative volumetric ratio of austenite to martensite was deducted using integrated intensity of respective phase according to direct comparison method [34]. The carbides of each coating and the reference material were extracted by an electrochemical anodic dissolution method as detailed elsewhere [36], and identified by both XRD and EDS. The hardness of specimens was measured using a Rockwell hardness tester and a micro-hardness tester. The wear scar was observed using the scanning electron microscope (SEM). The profile of the wear scar was measured along the direction perpendicular to wear direction, using DEKTAK^{3}ST surface profiler from the Sloan Technology. In some cases, wear scar was sectioned perpendicular to the clad tracks (i.e., perpendicular to wear direction) for metallographic observations.

3. Experimental Results

3.1. Microstructure of the Coatings

The carbides, identified using those extracted by electrochemical anodic dissolution method, are mainly vanadium-rich $(V, Cr)_8C_7$ (which is historically referred to as MC-type vanadium carbides [29, 37, 38]) for CPM 9V, 10V and 15V coatings, tungsten and molybdenum-rich M_6C for M4 coating, and chromium-rich M_7C_3 (Cr_7C_3) for D2. As shown in Fig. 1, XRD patterns indicate the presence of respective carbides in the coatings.

The as-clad CPM 9V coating shows typical dendritic microstructure (Fig. 2a), having a large proportion of retained austenite, as identified by the XRD pattern (Fig. 1a). The fraction of martensite is very limited, with a relative volumetric ratio of austenite to martensite being 8.5

(Table III). There is only a small fraction of lamellar eutectic carbides, existing in the interdendritic region (Fig. 2b). After post heat-treatment at 600°C, the retained austenite is mainly transformed to martensite (Fig. 1a and Table III). Meanwhile, the size and the fraction of the carbides seem to become marginally larger (Figs. 2c and 2d).

The as-clad CPM 15V coating contains a large proportion of primary carbides that are relatively big in size (about 2.3 μm), as shown in Figs. 3a and 3b. In addition, there is a significant proportion of idiomorphic "rod-like" eutectic carbides, fairly uniformly distributed in the matrix. Compared with CPM 9V, the fraction of retained austenite in CPM 15V is much smaller (Fig. 1c and Table III). Post heat-treatment at 600°C does not change much the microstructural feature (Fig. 3c), although the small fraction of retained austenite is transformed to martensite.

The M4 coating shows a mixture of cellular and dendritic structures (Figs. 4a and 4b). The carbides, being globular (average 0.6 μm in diameter) or rod-like, exist almost exclusively along the cell boundaries. The ratio of retained austenite to martensite of M4 coating is at the lowest level among the four coatings in as-clad condition (Table III). After post heat-treatment at 600°C, the retained austenite is transformed to martensite, with the size and distribution of the carbides remaining nearly unchanged (Figs. 4c and 4d).

Because of multiple overlapping clad-tracks, a thin layer of a clad track will be over-heated during depositing the next adjacent clad-track, forming a "re-heated zone" (RHZ) as shown schematically in Fig. 5. Depending on the type of the tool steel and processing parameters, there can be noticeable difference in microstructural features between the RHZ and the as-deposited clad track (ADCT). While the difference between the two areas is immaterial for the other three coatings, it is significant for the CPM 10V coating.

For the CPM 10V coating, eutectic structure prevails in the ADCT with fine rod-like eutectic carbides (Figs. 6a and 6b). Along the boundaries between eutectic regions, there is a thick band of martensite/retained austenite or their mixture, embedded with globular and rod-like carbides. In contrast, in the RHZ of CPM 10V coating, the carbides mostly are spherical in shape and uniformly distributed throughout the matrix (Figs. 6c and 6d). The ratio of the retained austenite to martensite is similar to that of the CPM 15V coating, much lower than that of the CPM 9V coating (Table III). The microstructural features in the ADCT and the RHZ remains almost unchanged after post heat-treatment at 600°C (Fig. 7). The carbides along the boundaries between eutectic regions tend to become more defined in the ADCT (Figs. 7a and 7b). The retained austenite is mostly transformed to martensite (Table III).

The coatings are free of cracks, according to visual examination of the original and ground surfaces as well as cross-sectional view using optical microscope and SEM. By comparison, the CPM 15V coating shows relatively more porosities (Fig. 3a), the size of which is small, less than 4 μm in their longest dimension. Other coatings have very limited amount of porosities and, if any, the size is very tiny (less than 1 μm as shown in Fig. 2b for the CPM 9V coating).

The D2 reference material has equiaxed microstructure as shown in Fig. 8. The size of chromium carbides is relatively large, with an average size of 11 μm and a maximum up to 30 μm.

3.2. Hardness and Wear Resistance of the As-Clad Coatings

The average hardness (of at least 8 measurements) of the as-clad coatings as well as the reference material (D2) is compared in Fig. 9. The volume loss during wear testing and the wear resistance of the as-clad coatings and the D2 steel are presented in Fig. 10a and Fig. 10b, respectively.

It can be seen from Fig. 10b that, in the as-clad condition, the CPM 15V coating exhibits the highest abrasive wear resistance among the tested materials. The CPM 9V coating is the least wear-resistant. Generally, the CPM 15V and CPM 10V coatings show superior abrasive wear resistance as compared with the reference material, D2, while the abrasive wear resistance of the CPM 9V and M4 coatings is inferior to that of the D2 steel.

The results also indicate that the hardness is not the direct measure of the abrasive wear resistance. The M4 coating, for example, while showing higher hardness than the D2 steel and the CMP 10V coating (Fig. 9), exhibits yet lower abrasive wear resistance (Fig. 10b).

3.3. Effects of Post Heat-Treatment on the Hardness and the Wear Resistance

The effects of post heat-treatment (tempering) on the hardness and the wear resistance of the coatings are shown in Figs. 11 and 12, respectively. For direct comparison purpose, the influence of post heat-treatment on wear volume loss is also compared in Fig. 12a. Generally, the post heat-treatment reduces the hardness and the abrasive wear resistance, except for the CPM 9V coating. In the case of the CPM 9V coating, after an initial drop when tempered at low temperatures, the hardness and the abrasive wear resistance of the coating increase with increasing heat-treatment temperature (Fig. 11 and Fig. 12b). After post heat-treated at 600°C, the wear resistance and the hardness of the coating become higher than those of the coating in the as-clad condition.

3.4. Localized Difference in the Wear Rate within One Coating

Fig. 13a shows the macroscopic parallel trails with regular peak-and-valley height changes on the wear scar of CPM 10V cladding. Obviously, the wear rate at valley is higher than that at the peak. Trails are parallel to the clad tracks, and the distance between two neighbouring peaks (or valleys) is exactly the same as the step-over used to move the laser beam from one track to the next during cladding process (1.75 mm for CPM 10V). This indicates that the peak-and-valley feature is a result of multiple overlapping clad-tracks. As shown in Fig. 13b, cross-sectional optical microstructure observation reveals that the valleys are correlated to the ADCT (with eutectic structure as identified in Fig. 6a) and that the peaks are correlated to the RHZ (with many uniformly distributed globular carbides as observed in Fig. 6c).

Fig. 14 shows the height difference between neighbouring peak and valley for all coatings. For CPM 10V, the height difference is very significant, indicating considerably different wear rate between the ADCT and the RHZ. Post heat-treatment further increases the difference. For other three coatings, in contrast, this difference in wear rate within the same coating is far less marked.

4. Discussion

For low-alloy steels, their hardness can usually serve as a measure of the abrasive wear resistance [28]. For tool steels containing a significant proportion of alloying elements and complex carbides, however, it was found that the wear resistance strongly depends on the proportion and type of the carbides [28]. For laser claddings of tool steels, the high cooling rate results in a microstructure with exceptional morphology of carbides and unique structure of matrix, as compared with that through conventional processing methods. The abrasive wear resistance of laser-clad coatings will depend integrally upon the features of carbides (including their type, proportion, shape, size and distribution) and the structure of the matrix. Although it is difficult to identify every factor separately due to the nature of complexity, in the following attempts are made to address each influencing factor with special cases, where one has a major role to play.

4.1. Effects of the Carbide Proportion

The volume proportion of carbides plays an important role in the wear resistance. For the CPM 9V, 10V and 15V coatings, for example, since they belong to a family containing the same type of vanadium-rich carbides, a coating with higher volume fraction of carbides exhibits higher wear resistance, which correlates also with higher hardness.

The CPM 15V coating has a large proportion of carbides, providing efficient resistance against scratching. As shown in Fig. 15a, the wear scar of the coating is pretty even with no scratching appearance. Fairly uniformly distributed large primary carbides are standing out against the worn surface, effectively reducing the wear rate.

The CPM 9V coating, on the other hand, contains a low fraction of carbides, with a matrix having low hardness due to the large proportion of retained austenite. As a result, the material is easily scratched away during the wear testing. Relatively deep scratching marks can be seen on the wear scar of the coating (Fig. 15b). The abrasive wear resistance of the coating is low.

Compared with the CPM 9V, the CPM 10V coating possesses larger volume proportion of carbides, which, combined with smaller fraction of retained austenite, enables the coating to have higher abrasive resistance. Compared with the CPM 15V, however, the CPM 10V coating has even lower volumetric ratio of retained austenite to martensite (Table III). It is because of the smaller proportion of carbides that results in the lower wear resistance of the CPM 10 coating than that of the CPM 15V coating.

4.2. Effects of the Carbide Shape and Distribution

The different wear rate between the ADCT and the RHZ cannot be explained from the hardness point of view, as the microhardness exhibits no measurable difference between the two zones (Fig. 16). The difference is attributed to the considerable distinction in the shape and distribution of the carbides in these two zones.

In the ADCT, the rod-like eutectic carbides are relatively easy to be broken and pulled out during the wear testing, resulting in tiny hole-like features and an uneven appearance on the wear scar (Fig. 17a). Moreover, along the boundaries between the eutectic regions, although the carbides are larger and many of them are globular, they are distributed non-uniformly. In regions where no carbides are present, martensite/retained austenite is easy to be scratched away locally. As soon as the

surrounding matrix is worn off, isolated carbides embedded in the boundaries are easily pulled out. The loosen carbides can further scuff the surrounding matrix. Such processes are clearly demonstrated by the small holes observed on the wear scar of the ADCT.

In the RHZ, globular carbides are evenly distributed in the matrix, and all of them are equally effective against scuffing. As a result, the wear scar is fairly even in this area (Fig. 17b). Assuming that there is no significant difference in volume fraction of the carbides between these two areas, it is obvious that the efficiency of the carbides against scratching is significantly higher in the RHZ, resulting in much higher wear resistance in the RHZ as compared with that in the ADCT.

4.3. Effects of the Carbide Size and Type

In spite of its higher hardness, the M4 coating exhibits lower wear resistance compared with both the D2 reference material and the CPM 10V coating. This is also attributed to the carbides, especially to the effects of their type and size.

For the D2 reference material, notable scratching marks can be observed on the wear scar in the matrix area (Fig. 18), indicating that the matrix is not so scratching-resistant. However, the scratching marks are interrupted at the location of the chromium carbides (see location A in Fig. 18). Because of their large size, the chromium carbides offer relatively high localized resistance against scratching and are difficult to be ploughed away, providing local "anti-wear islands" and increasing overall abrasive wear resistance.

The W and Mo-rich M_6C should be harder and have higher wear resistance as compared with Cr_7C_3 [28]. However, the W and Mo-rich M_6C-type carbides in the M4 coating are relatively tiny in size (average 0.6 μm in diameter), which can be scratched away much more easily, providing less resistance to abrasion, as compared with the large chromium carbides in the D2 tool steel. As shown in Fig. 19, the scratching lines, many of which are wider than the size of the carbides, are continuous in nature, although a relatively large amount of small carbides are present in the way.

The size of carbides in the M4 coating is comparable with that in the CPM 10V coating (with an average dimension of about 0.6 μm in the M4 coating and in the RHZ of the CPM 10V coating). However, the V-rich carbides in the CPM 10V coating are harder and more wear-resistant than Mo- and W-rich M_6C-type carbides in the M4 coating [28, 30]. No remarkable scratching marks can be seen on the wear scar of the CPM 10V coating. In addition, the volume fraction of carbides in the M4 coating is lower than that in the CPM 10V coating. Therefore, even with higher overall hardness, the wear resistance of the M4 coating is inferior to that of the CPM 10V coating.

4.4. Effects of the Matrix

For all coatings, post heat-treatment may increase the proportion of the carbides slightly, while retaining their type and morphology. This alone should lead to an increase in wear resistance. Obviously, the decrease in the hardness and the wear resistance of the CPM 10V, 15V and M4 coatings after post heat-treatment is due to the tempering effect, which reduces the hardness and, therefore, the scratching resistance of the matrix.

Unlike other coatings, the CPM 9V coating shows a unique response to the post heat-treatment. This is attributed to its large proportion of retained austenite in the "as-clad" condition. The retained austenite will be transformed to martensite at elevated temperatures whenever kinetically possible [14, 15]. This phase transformation will increase the hardness of the matrix and, hence, the overall wear resistance. According to the current study, the transformation begins at a temperature as low as 260°C (Table III), and the degree of the phase transformation increases with increasing heat-treatment temperature. At low temperatures (below about 400°C), the tempering effect on the matrix (as observed in other coatings) prevails, the hardness and the wear resistance of the coating after post heat-treatment become lower. When heat-treating at higher temperatures (above about 400°C), on the other hand, the effect of the phase transformation of retained austenite to martensite is significant enough to offset the tempering effect, resulting in higher hardness and wear resistance of the coating than those of the coating in the as-clad condition.

For the CPM 10V, 15V and M4 coatings, the volume fraction of retained austenite is much smaller than that of the CPM 9V coating. The increase in the hardness and the wear resistance due to the phase transformation of retained austenite to martensite is insignificant as compared with the decrease in them due to the tempering effect on the matrix.

5. Conclusions

By pre-heating the substrate, cracking-free thick coatings of CPM 9V, 10V, 15V and M4 tool steels have been deposited on carbon steel substrates by laser cladding process. Detailed studies of the abrasive wear behaviour of these coatings with a sand/rubber wheel test machine have been conducted and the following conclusions can be drawn:

1. The abrasive wear resistance of the laser-clad CPM 15V and CPM 10V coatings is superior to that of the D2 steel, while the wear resistance of the CPM 9V and M4 coatings is inferior to that of the D2.
2. During multi-track cladding, a thin layer of a pre-deposited clad track can be over-heated by depositing the next adjacent one, resulting in a re-heated zone with different wear rate compared with the area of the track in the as-clad condition. This effect is especially significant for the CPM 10V coating, while minor for the CPM 9V, 15V and M4 coatings.
3. The abrasive wear resistance of tool steel coatings is dependent on both the matrix microstructure and the features of dispersed carbides.
4. In terms of dispersed carbides, their type, proportion, shape, size, and distribution are the determining factors for the abrasive wear resistance of the tool steel coatings.
5. When a large proportion of retained austenite exists in the coating, the wear resistance can be improved through the transformation of the retained austenite to martensite promoted by post heat-treatment.

Acknowledgements

The authors are indebted to J. Fenner for preparing the wear specimens and to M. Meinert for the assistance in materials characterization. Thanks are also due to M. U. Islam, the director of the Production Technologies Research Program of IMTI, for his technical review and critical comments on the manuscript.

References

1. V. M. Weerasinghe, W.M. Steen, Proceeding of the First International Conference on Lasers in Materials Manufacturing, Brighton, UK, 1983, p. 125.
2. W.M. Steen, Proceeding of the Conference on Laser Surface treatment of Metals, San Miniato, Italy, 1985, p. 369.
3. K. Komvopoulos, K. Nagarathnam, Journal of Engineering Materials and Technology, 112 (1990) 131.
4. A.F.A Hoadley, A. Frenk, C. F. Marsden, Surface Engineering: Processes and Application, Technomic Publishing Co., Inc., Lancaster, PA, 1995, p. 171.
5. L. Pawlowski, Journal of Thermal Spray Technology, 8 (1999) 279.
6. R. Vilar, International Journal of Powder Metallurgy, 37 (2001) 31.
7. A. Wetzig, B. Brenner, V. Fux, E. Beyer, Laser Materials Processing, Vol. 85, Laser Institute of America, Orlando, USA, 1998, Section D – ICALEO 1998, p. 20.
8. J.M. Yellup, Surface and Coatings Technology, 71 (1995) 121.
9. I.S. Batra, C.S. Viswanadham, V. Sethumadhavan, D.N. Sah, C.L. Goswami, N.G. Kakovkina, D.M. Gureyev, Trans. Indian Inst. Met., 45 (1992) 81.
10. R. Colaço, C. Pina, R. Vilar, Scripta Materialia, 41 (1999) 715.
11. R. Colaço, R. Vilar, Journal of Materials Science Letters, 17 (1998) 563.
12. R. Colaço, R. Vilar, Surface Engineering, 12 (1996) 319.
13. R. Colaço, R. Vilar, Scripta Materialia, 36 (1997) 199.
14. R. Colaço, R. Vilar, Rev. Metal. Madrid, 34 (1998) 135.
15. R. Colaço, R. Vilar, Scripta Materialia, 38 (1998) 107.
16. C.T. Kwok, K.I. Leong, F.T. Cheng, H.C. Man, Materials Science and Engineering A, 357 (2003) 94.
17. L. Åhman, Metallurgical Transactions A, 15A (1984) 1829.
18. Y. W. Kim, P.R. Strutt, H. Nowotny, Metallurgical Transactions A, 10A (1979) 881.
19. P.A. Molian, H.S. Rajasekhara, Journal of Materials Science Letters, 5 (1986) 1292.
20. P. R. Strutt, Met. Forum, 4 (1981) 117.
21. P.R. Strutt, H. Nowotny, Materials Science and Engineering, 36 (1978) 217.
22. H.J. Niu and I.T.H. Chang, Metallurgical and Materials Transactions A, 31A (2000) 2615.
23. Y. Hu, C. Chen, K. Mukherjee, Materials and Manufacturing Processes, 13 (1998) 369.
24. Y. Zhang, X. Yuan, X. Zeng, ICALEO 1999: Laser Materials Processing Conference, San Diego, USA, 1999, p. 241.
25. J. R. Davis (Ed.), "Surface Engineering of Tool and Die Steels", ASM Specialty Handbook: Tool Materials, ASM international, Materials Park, OH, 1995, p. 383.
26. Y. Zhang, X. Zeng, X. Yuan, ICALEO 2001: Applications of Lasers & Electro-Optics, Jacksonville, USA, 2001, p. 577.
27. W. Stasko, K.E. Pinnow, European Patent: EP 0515018A1, 1992.
28. E. Tarney, Stamping Quarterly, 8 (1996) 18.
29. A. Kasak, E.J. Dulis, Powder Metallurgy, 21 (1978) 114.
30. R.W. Bratt, Met. Powder Rep., 38 (1983) 475.
31. W. Stasko, K.E. Pinnow, R.B. Dixon, Proceeding of the 5th International Conference on Advanced Particulate materials and Processes, Metal Powder Industries Federation, Princeton, NJ, 1997, p. 401.
32. E.J. Dulis, J.H. Moll, W. Stasko, Key Engineering Materials, 77-78 (1993) 263.

33. W. Stasko, K.E. Pinnow, W.B. Eisen, Proceeding of the Confereence on Advances in Powder Metallurgy and Particulate Materials-1996, Vol. 5, Metal Powder Industries Federation, Princeton, NJ, 1996, p. 17.179.
34. J.-Y. Chen, S.-H. Wang, L. Xue, Proceeding of the 3rd International Surface Engineering Congress, ASM International, August 2-4, 2004, Orlando, Florida (in press).
35. A.L. Greer, K.L. Rutherford, I.M. Hutchings, International Materials Reviews, 47 (2002) 87.
36. L. Xue, A.Theriault, J.Y. Chen, M.U. Islam, A. Wieczorek, G. Draper, Proceeding of the 10th International Symposium on Processing and Fabrication of Advanced Materials X, ASM International, Materials Park, 2002, p. 361.
37. M. Boccalini, H. Goldenstein, International Materials Reviews, 46 (2001) 92
38. T. Okane, T. Umeda, Int. J. Cast Metals Res., 11 (1999) 291.

Figure Captions

Fig. 1: X-ray diffraction patterns of the coatings in the as-clad condition and after post heat-treatment at temperatures indicated in the plots (a: CPM 9V; b: CPM 10V; c: CPM 15V; d: M4).

Fig. 2: SEM micrographs showing the representative microstructures of CPM 9V coatings (a & b: in the as-clad condition; c & d: after post heat-treatment at 600°C).

Fig. 3: SEM micrographs showing the representative microstructures of CPM 15V coatings (a & b: in the as-clad condition; c: after post heat-treatment at 600°C).

Fig. 4: SEM micrographs showing the representative microstructures of M4 coatings (a & b: in the as-clad condition; c & d: after post heat-treatment at 600°C).

Fig. 5: Schematic representation of the cross-sectional view of multiple overlapping clad tracks, showing the areas of the tracks in the as-clad condition (the "as-deposited clad track", ADCT) and the over-heated areas in the tracks during depositing the next adjacent ones (the "re-heated zone", RHZ).

Fig. 6: SEM micrographs showing the representative microstructures of the CPM 10V coating in the as-clad condition (a & b: ADCT; c & d: RHZ).

Fig. 7: SEM micrographs showing the representative microstructures of the CPM 10V coating after post heat-treatment at 600°C (a & b: ADCT; c & d: RHZ).

Fig. 8: SEM micrograph showing the representative microstructures of conventionally hardened D2 tool steel.

Fig. 9: Comparison of the hardness of the as-clad coatings and the D2 reference material.

Fig. 10: Comparison of (a) the volume loss during wear testing, and (b) the wear resistance of the as-clad coatings and the D2 reference material.

Fig. 11: Influence of post heat-treatment on the hardness of the coatings.

Fig. 12: Influence of post heat-treatment on (a) the volume loss during wear testing, and (b, c, d) the wear resistance of the coatings.

Fig. 13: Regular peak-and-valley trails on the wear scar of the as-clad CPM 10V coating (a), and optical micrograph of cross-sectional view of the wear scar, showing different wear rate between the ADCT and the RHZ (b).

Fig. 14: Effect of post heat-treatment on the height difference between the peak and the valley on wear scars of the coatings.

Fig. 15: SEM micrographs showing the characteristic morphology of wear scars (a: as-clad CPM 15V coating; b: as-clad CPM 9V coating).

Fig. 16: Microhardness measured perpendicular to the clad track of the CPM 10V coating, showing no significant difference between the ADCT and the RHZ.

Fig. 17: SEM micrographs showing the characteristic morphology at different locations of the wear scar of the CPM 10V coating (a: at the "valley" - ADCT; b: at the "peak" - RHZ).

Fig. 18: SEM micrograph showing the characteristic morphology of the wear scar of conventionally hardened D2 tool steel (Location *A*: individual carbide relatively large in size providing high local scratching resistance).

Fig. 19: SEM micrograph showing the characteristic morphology of the wear scar of the M4 coating.

Table I: Compositions of the Experimental Materials (wt.%)

	C	*V*	*Cr*	*Mo*	*Mn*	*Si*	*W*	*S*	*Fe*
CPM 9V	1.78	9.00	5.25	1.30	0.50	0.90	-	-	Balance
CPM 10V	2.45	9.75	5.25	1.30	0.50	0.90	-	<0.09	Balance
CPM 15V	3.40	14.50	5.25	1.30	0.50	0.90	-	0.07	Balance
M4	1.45	3.9	4.5	4.5	-	-	5.8	0.12	Balance
D2	1.50	1.00	12.00	1.00	-	-	-	-	Balance
AISI 1070	0.69	-	-	-	0.68	0.38	-	0.04	Balance

Table II: Parameters for laser cladding

	CPM 9V	*CPM 10V*	*CPM 15V*	*M4*
Laser beam power (kW)	2.5	2.5	3	2.75
Laser beam diameter (mm)	2	2	2	2
Substrate traverse speed (mm/s)	7.6	7.6	8.6	8.6
Powder feed rate (g/min)	20	16	11	9
Overlap (%)	30	30	30	50

Table III: Relative volumetric ratios of retained austenite to martensite

	CPM 9V	*CPM 10V*	*CPM 15V*	*M4*
As-clad coating	8.5	1.3	1.5	0.26
After heat-treatment at 260°C	7.9	1.1	1.4	0.17
After heat-treatment at 400°C	0.6	0.6	1.3	0.17
After heat-treatment at 600°C	0.2	0.1	0	0

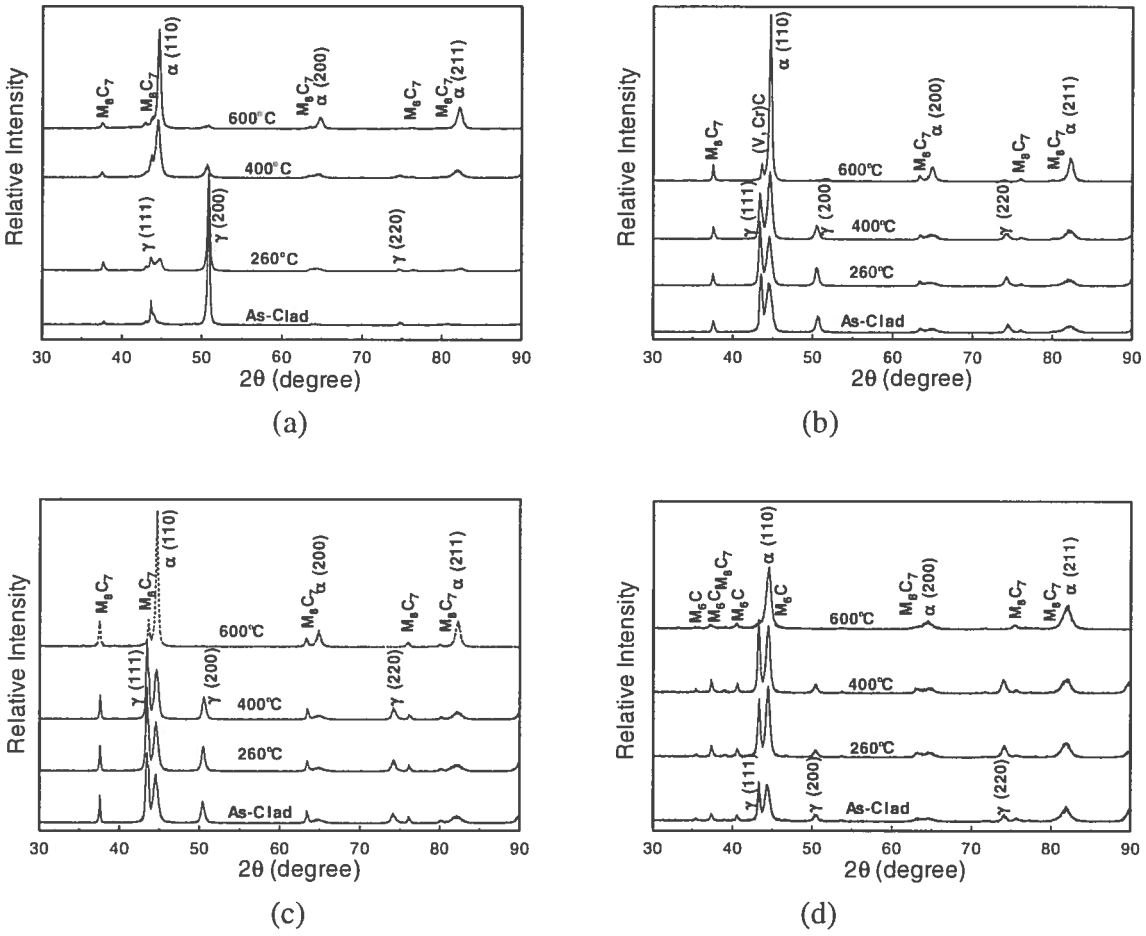
Relative Intensity
2θ (degree)
600°C
400°C
260°C
As-Clad
M_6C_7
α (110)
α (200)
α (211)
γ (111)
γ (200)
γ (220)
(a)
600℃
400℃
260℃
(V,Cr)C
(b)
(c)
M_6C
(d)

Fig. 1

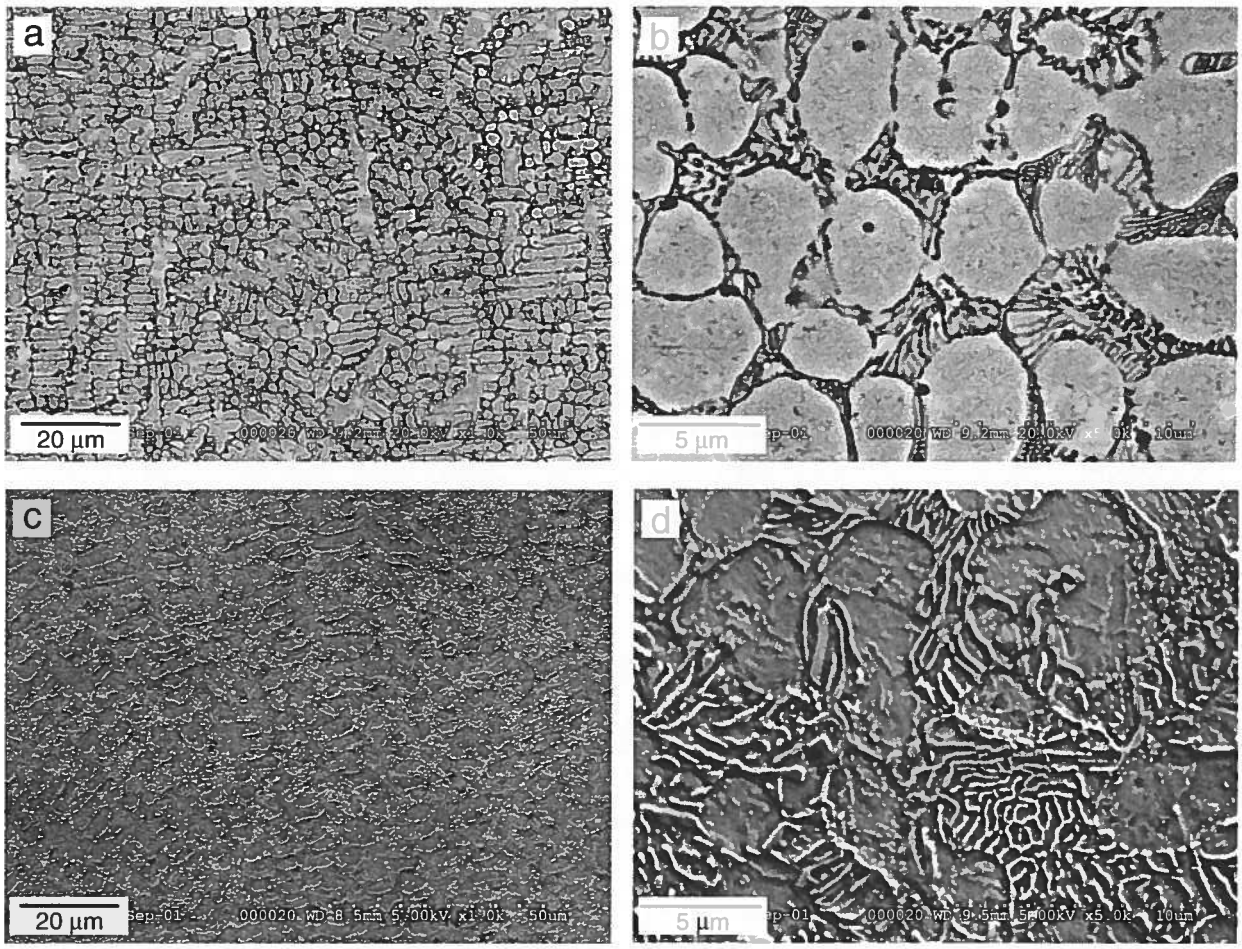

Fig. 2

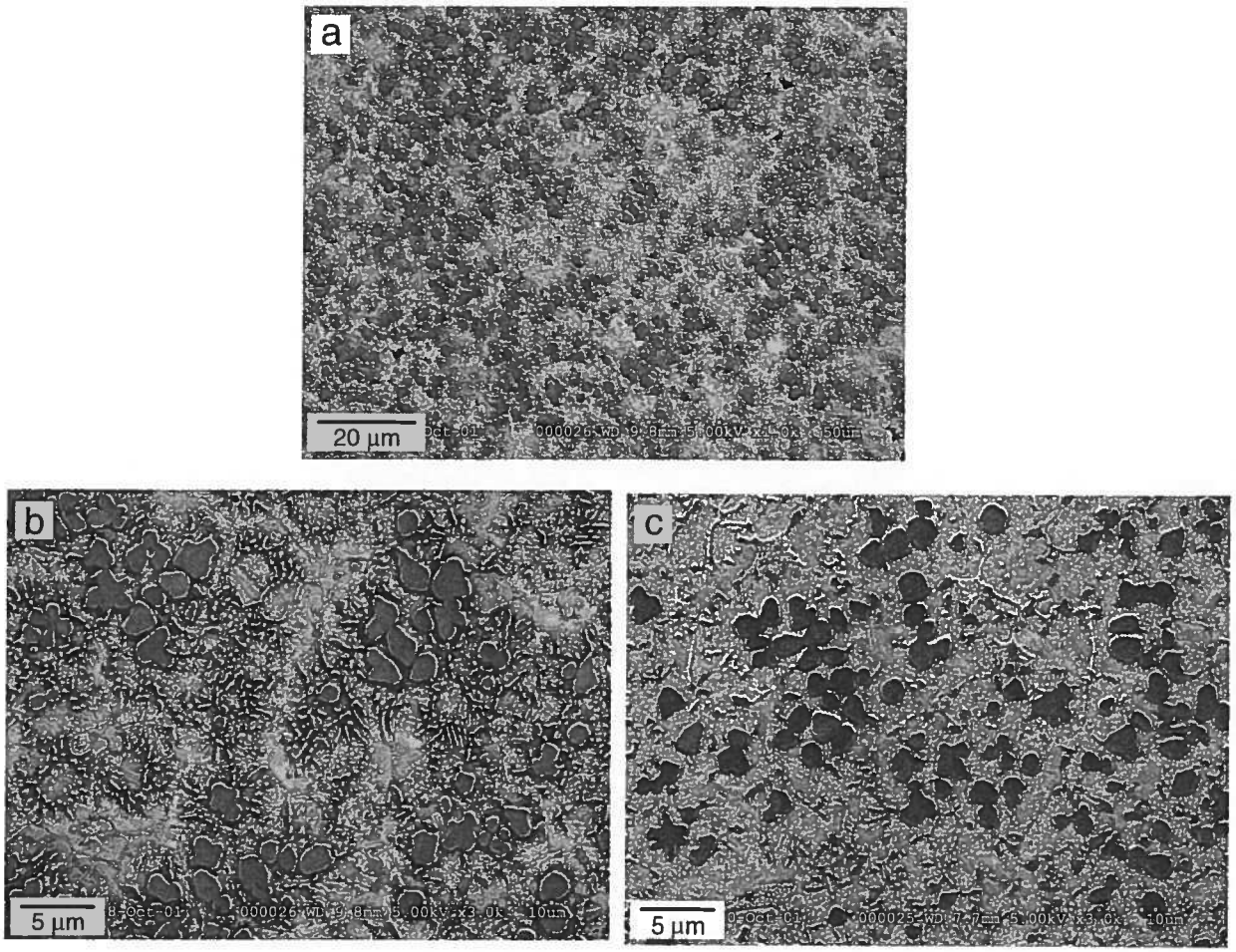

Fig. 3

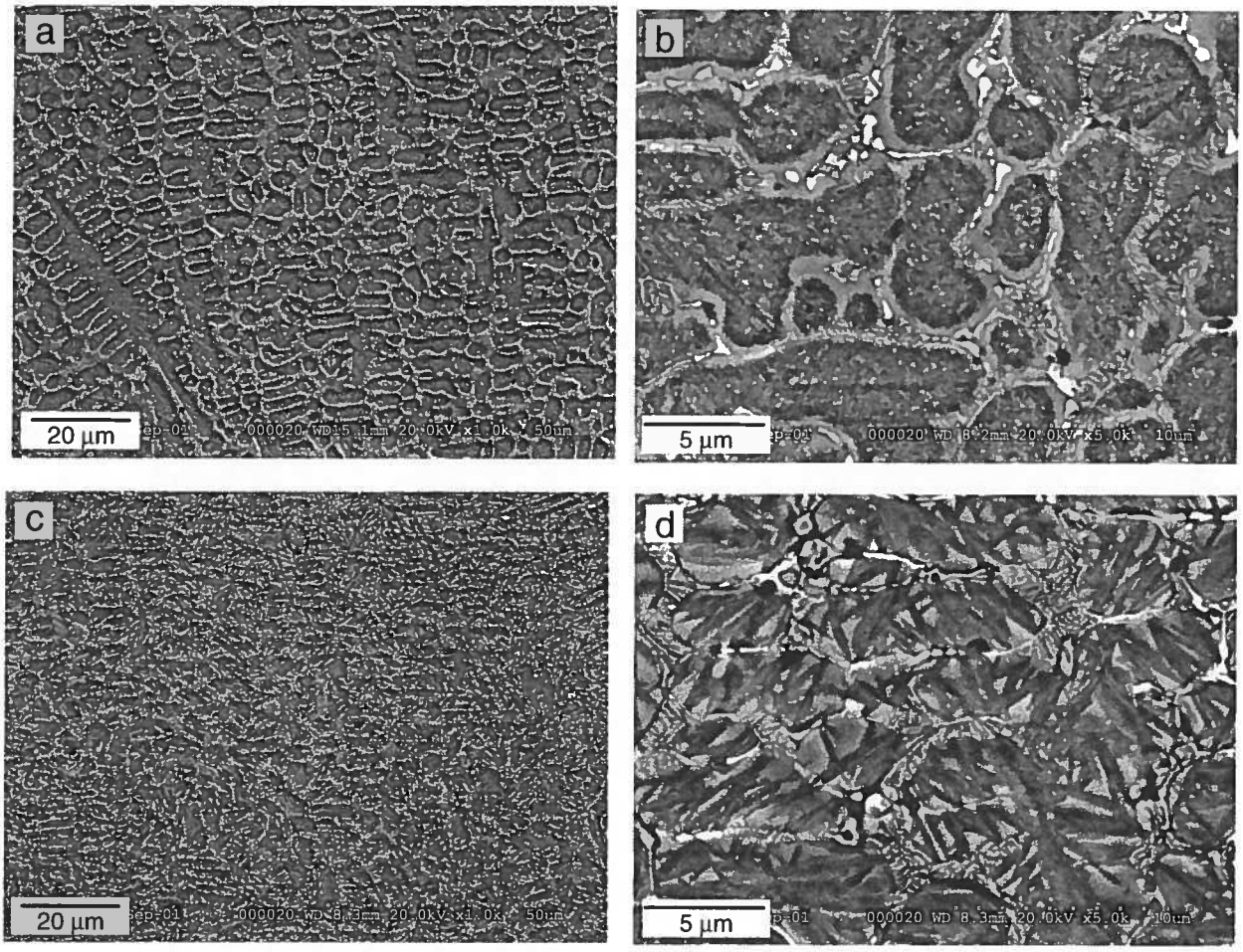

Fig. 4

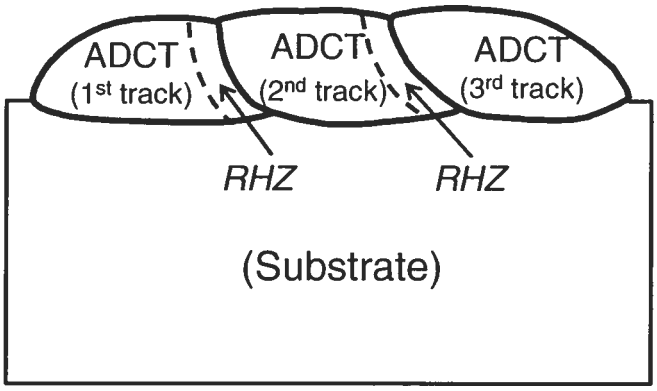
ADCT
(1st track)
ADCT
(2nd track)
ADCT
(3rd track)
RHZ
RHZ
(Substrate)

Fig. 5

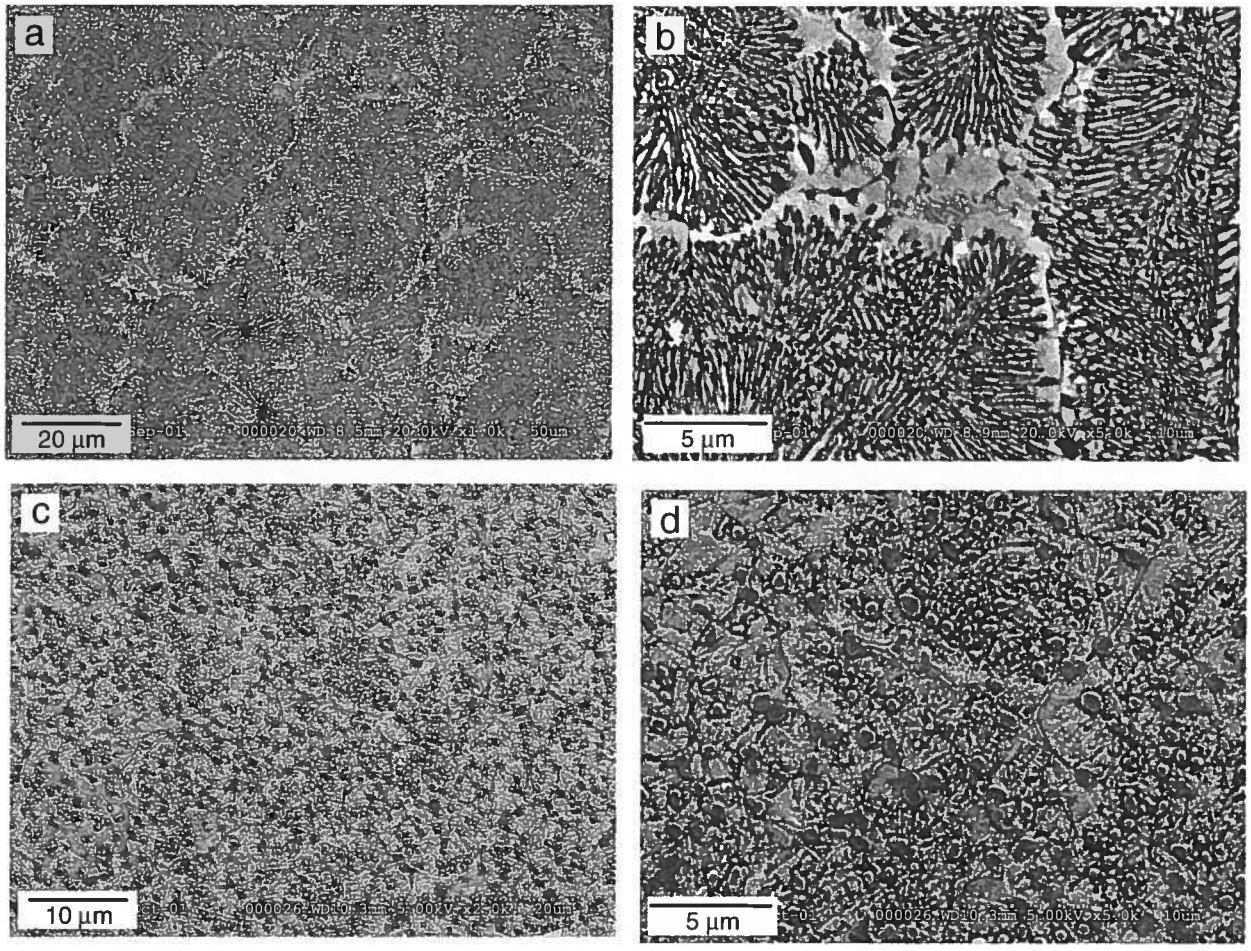

Fig. 6

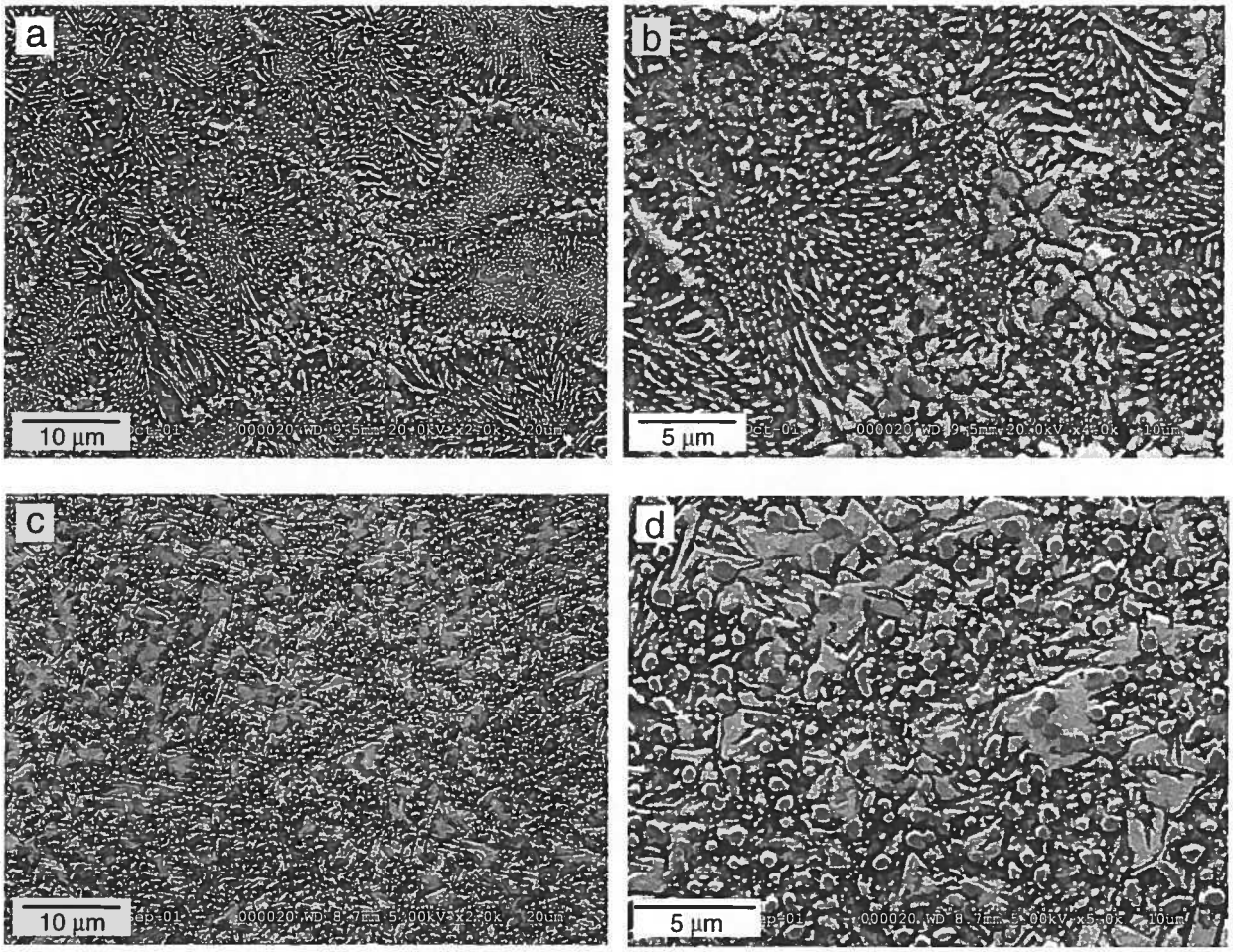

Fig. 7

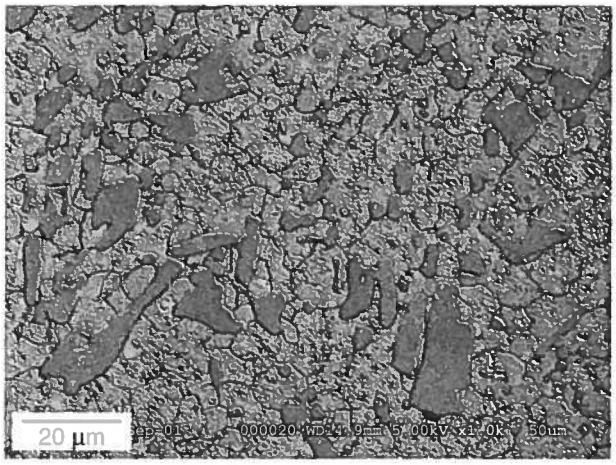

Fig. 8

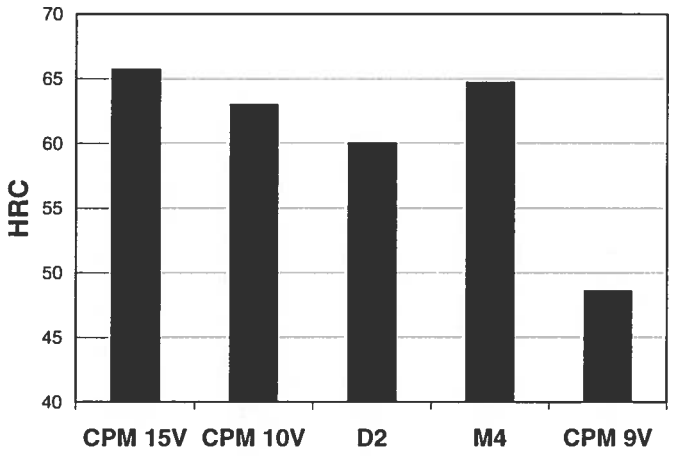

Fig. 9

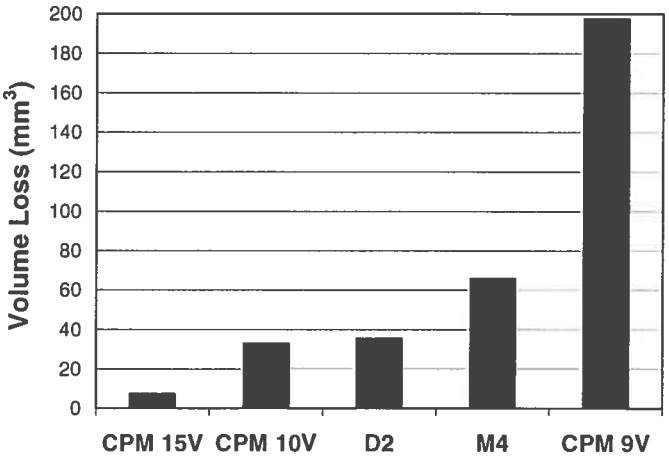
Volume Loss (mm3)
200
180
160
140
120
100
80
60
40
20
0
CPM 15V
CPM 10V
D2
M4
CPM 9V

(a)

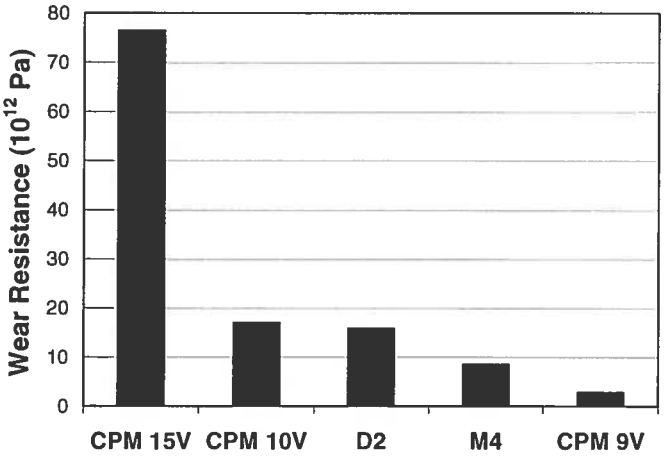
Wear Resistance (10^12 Pa)
80
70
60
50
40
30
20
10
0
CPM 15V
CPM 10V
D2
M4
CPM 9V

(b)

Fig. 10

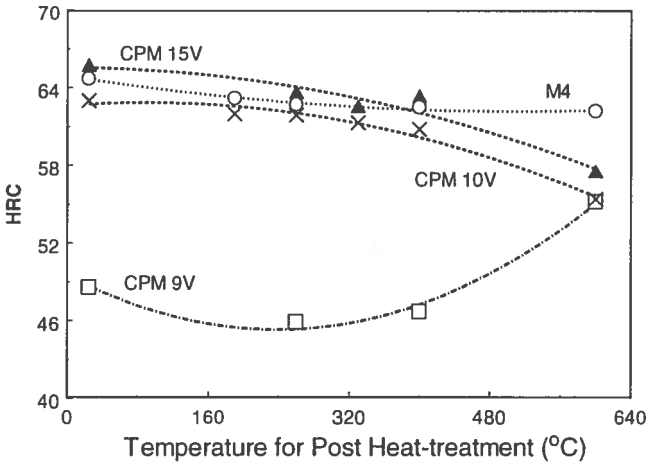
70
64
58
52
46
40
HRC
CPM 15V
M4
CPM 10V
CPM 9V
0
160
320
480
640
Temperature for Post Heat-treatment (°C)

Fig. 11

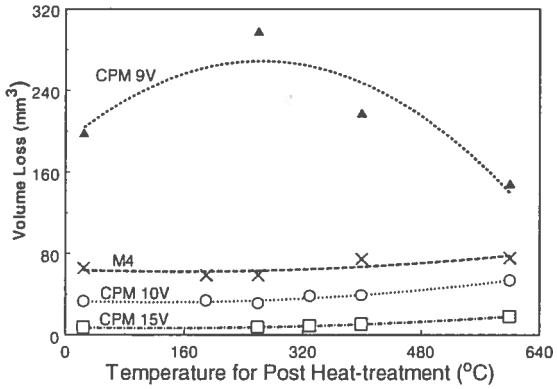
CPM 9V
M4
CPM 10V
CPM 15V
Volume Loss (mm3)
Temperature for Post Heat-treatment (°C)

(a)

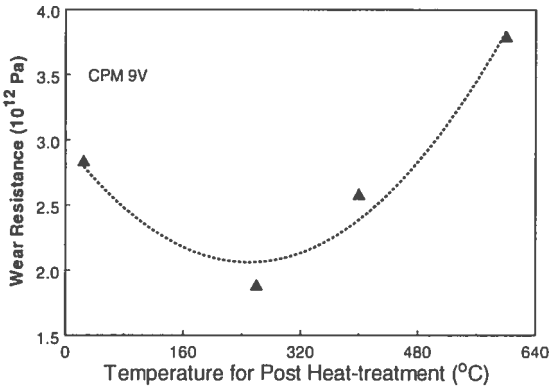
CPM 9V
Wear Resistance (10^12 Pa)
Temperature for Post Heat-treatment (°C)

(b)

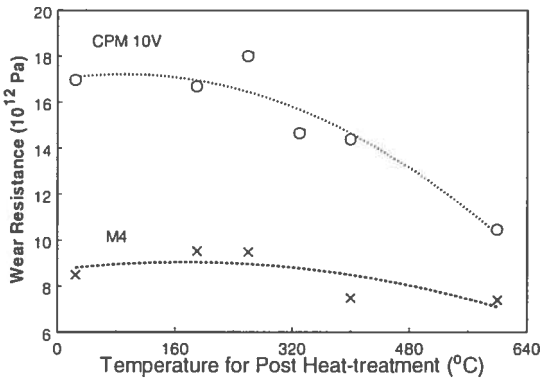
CPM 10V
M4
Wear Resistance (10^12 Pa)
Temperature for Post Heat-treatment (°C)

(c)

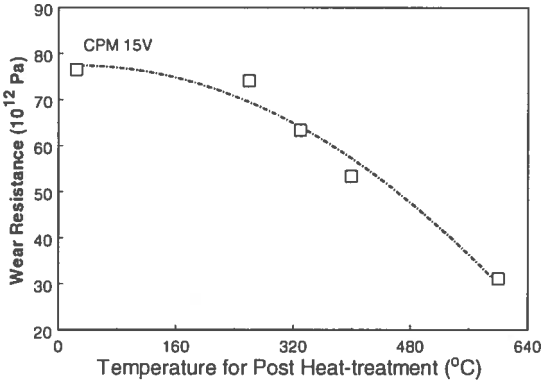
CPM 15V
Wear Resistance (10^12 Pa)
Temperature for Post Heat-treatment (°C)

(d)

Fig. 12

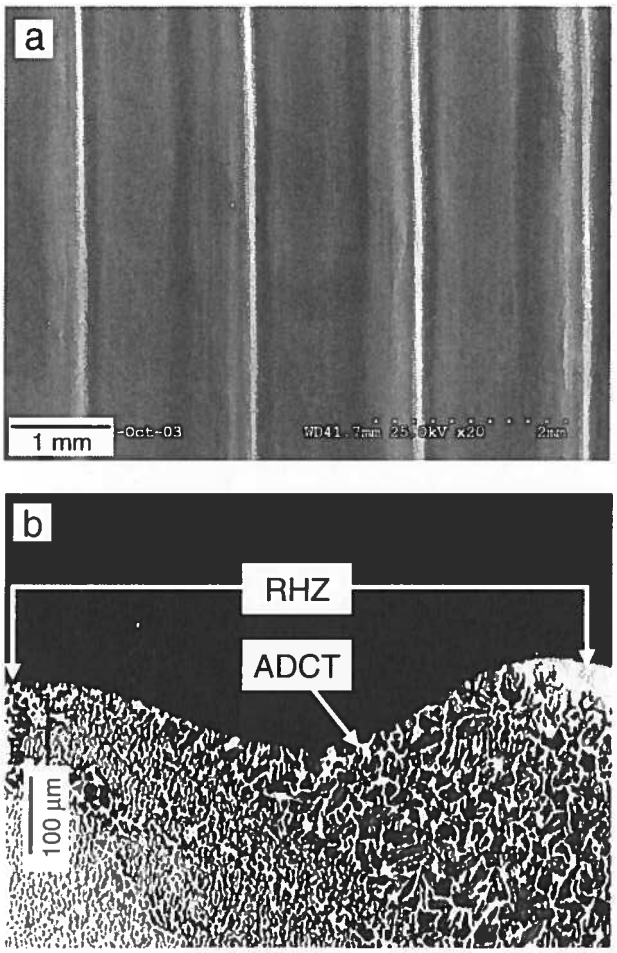

Fig. 13

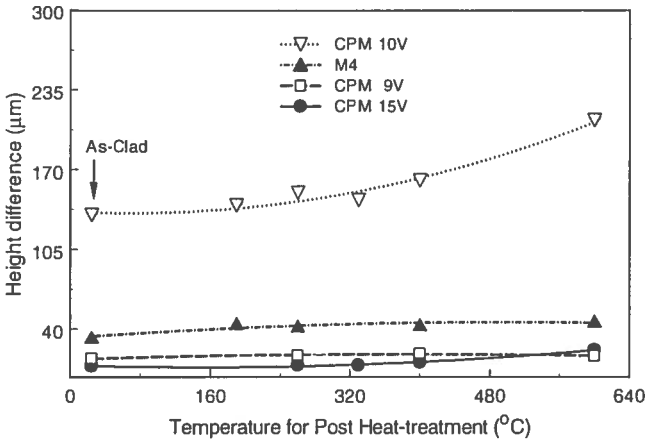
300
235
170
105
40
Height difference (μm)
CPM 10V
M4
CPM 9V
CPM 15V
As-Clad
0
160
320
480
640
Temperature for Post Heat-treatment (°C)

Fig. 14

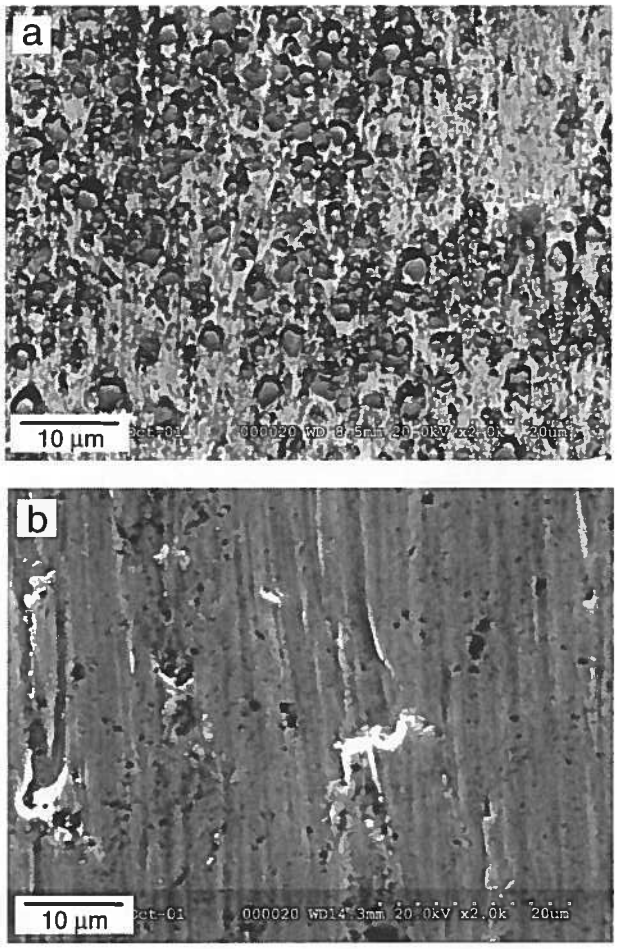

Fig. 15

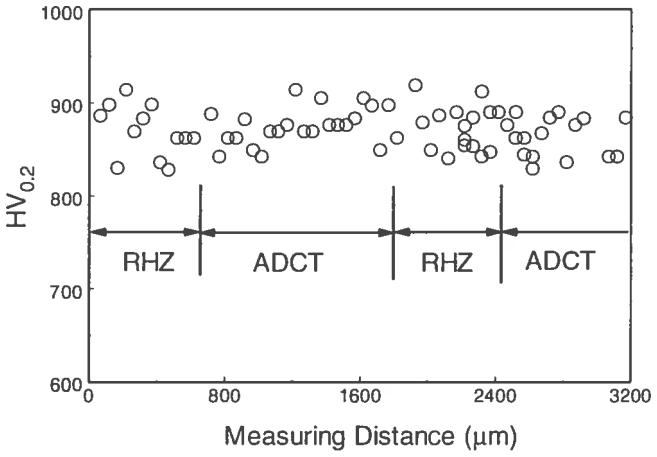
1000
900
800
700
600
$HV_{0.2}$
RHZ
ADCT
RHZ
ADCT
0
800
1600
2400
3200
Measuring Distance (μm)

Fig. 16

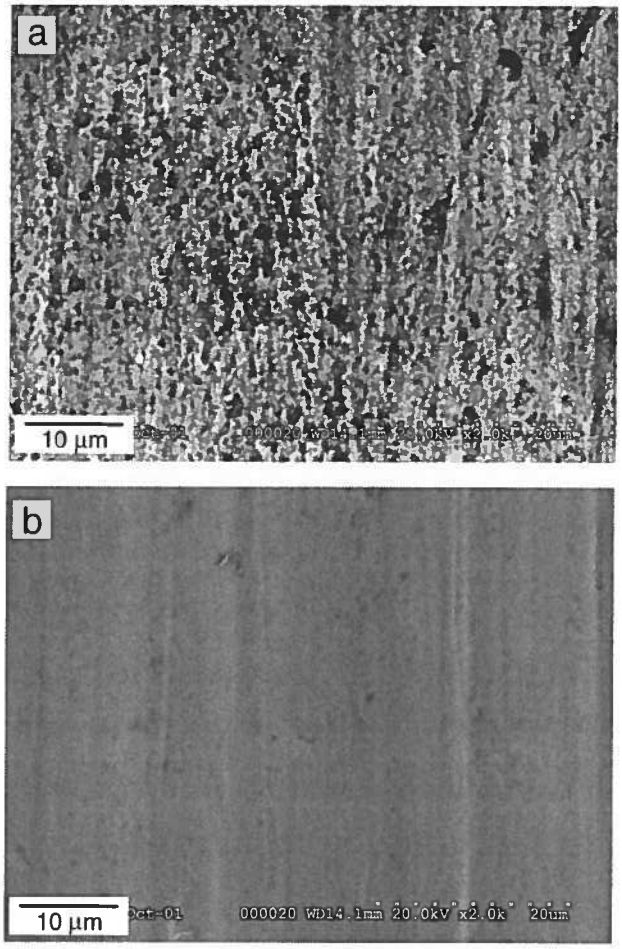

Fig. 17

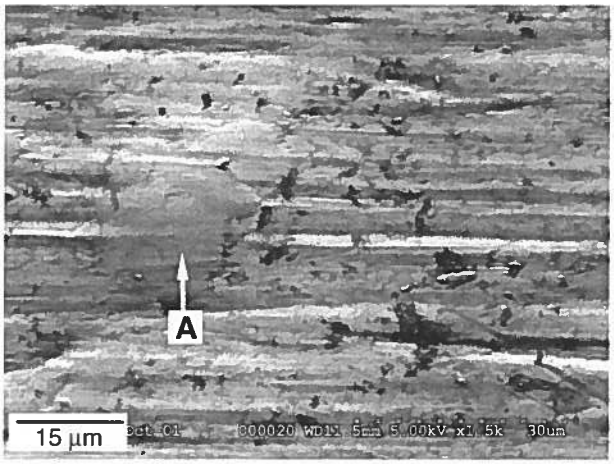

Fig. 18

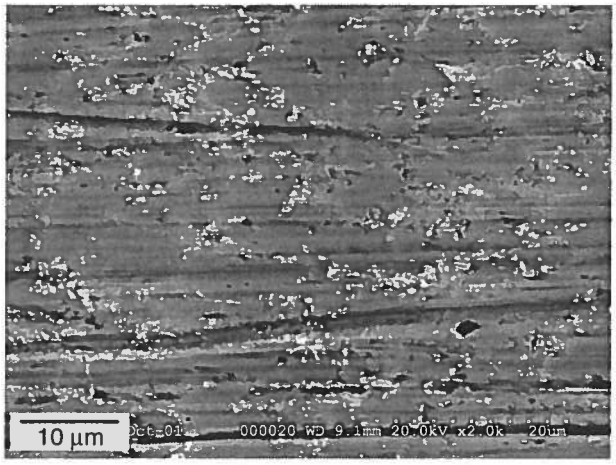

Fig. 19